Characterization of Surface Cracks Using Eddy Current NDT Simulation by 3D-FEM and Inversion by Neural Network

B. Helifa [1], M. Féliachi [2], I. K. Lefkaier [1], F. Boubenider [3], A. Zaoui [4], and N. Lagraa [5]

[1] Laboratoire de Physique des Matériaux
Université de Laghouat, BP 37G, Laghouat 03000, Algérie
helifa@yahoo.fr, lefkaier_ik@yahoo.fr

[2] IREENA-IUT
Université de Nantes – L'UNAM, CRTT, BP 406, 44602 Saint-Nazaire cedex, France
mouloud.feliachi@univ-nantes.fr

[3] Laboratoire de Physique des Matériaux
USTHB, Bab-Ezzouar, Alger 016000, Algérie
fboubenider@hotmail.com

[4] EMP
BP 17 Bordj El Bahri 16100 Alger, Algérie
zaoui_abdelhalim@yahoo.fr

[5] Laboratoire d'Informatique et de Mathématique
Université de Laghouat, BP 37G, Laghouat 03000, Algérie
nasrlag@gmail.com

Abstract ─ In this work, we suggest an approach of signal inversion from sensors used in eddy current (EC) nondestructive testing (NDT). The aim is to characterize surface cracks from the EC signal. A methodology that combines 3D finite element (FEM) simulation and a data inversion by neural networks (NN) is proposed. We show that the use of a set of numerical measurements representing the EC signature of surface crack enables to remedy of the unicity problem. The obtained results show that the developed approach leads to the quantification of the crack.

Index Terms ─ 3D finite element simulation, eddy current NDT, neural network, surface cracks.

I. INTRODUCTION

Non-destructive testing by eddy currents is a powerful tool for testing the quality and reliability. Its exploiting in real-time has become a capital necessity, and it is essential to have a fast mean for the inversion of eddy current signals.

Usually, this inversion is carried out through an experimental investigation by plotting the standard curves, which is efficient but costly investigation [1], or through an optimization algorithm leading to a computation time that can easily become prohibitively high [2], [3], [4] and [5].

In this context, 3D finite element simulation is performed in order to construct a database relating the sensor impedance variation and the crack geometry, which will be used instead of experimental measurements. After that, data inversion by means of neural networks is performed and enables us to fully characterize the surface crack. In this approach, the obtained signal represents the no perturbed crack one. Therefore, the use of wavelet and IFT techniques cannot give any addition, since they are usually performed in perturbed environment [6], [7], [8] and [9]. In this work, we test the validity of obtained results by comparing them with experimental ones in "Team Workshop Problem 15" [10].

II. MODELING

Eddy current NDT system can be modeled by the scheme represented in Fig. 1. A material representing the critical part and containing the crack is subjected to the action of an electromagnetic field produced by a coil forming the EC sensor where a time-changing current density is imposed.

The aim is to evaluate the eddy currents in the

defective part and the change in impedance of the coil.

Our simulation of the EC NDT devices is carried out in the context of harmonic quasi-stationary regime.
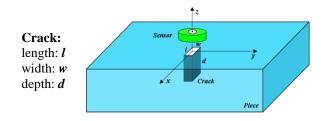

Crack:
length: l
width: w
depth: d

Fig. 1. Sensor-crack system.

Amongst the usual formulations in use for the EC problem, the « $\vec{A}V - \vec{A}$ » nodal formulation is the most popular due to its generality, robustness and ease of implementation without any restriction on continuity conditions [11].

The adopted formulation of the 3D electromagnetic model is:

$$\begin{cases} \vec{\nabla} \times \nu\vec{\nabla} \times \vec{A} - \vec{\nabla}\nu\vec{\nabla} \cdot \vec{A} + \sigma\left(\dfrac{\partial \vec{A}}{\partial t} + \vec{\nabla} \cdot V\right) = \vec{J}_s \\ \vec{\nabla} \cdot \sigma\left(\dfrac{\partial \vec{A}}{\partial t} + \vec{\nabla} \cdot V\right) = 0. \end{cases} \quad (1)$$

The geometry and the meshing are developed using GMSH mesher [12].

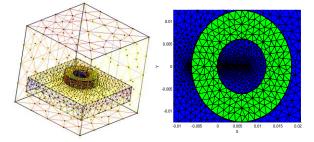Figure 2 shows a part of the meshing of the system.

Fig. 2. Top view of the meshing of the system generated by GMSH.

Our study is based on data analysis of scans, carried out by small displacements of the sensor with 0.5 mm or 1 mm steps, parallel and perpendicular to the crack on the surface of the material. In order to simulate the movement of the sensor, while keeping the same mesh topology, we use the 3D band geometry method [13]. The obtained results will be compared to experimental data of the academic benchmark configuration [10].

III. EDDY CURRENT REPRESENTATION

In every position of the sensor on the surface of material, we calculate both the impedance of the system with and without the crack. The impedance variation ΔZ is given by:

$$\Delta Z = \frac{j\omega}{I^2} \int_{\Omega_s} \left(\vec{A} - \vec{A}_0\right) \cdot \vec{J}_s \, d\Omega_s, \quad (2)$$

where $\vec{A}$ and $\vec{A}_0$ are the magnetic vector potentials with and without the crack respectively; I and ω are respectively the intensity and the frequency of the current in the coil; Ω_s is the volume of the coil. We note here that, the integral in the above equation corresponds to the electromagnetic energy difference in the coil with and without the crack, so the simulation of the case "zero" (no cracks) is always included.

Figure 3 shows the EC signals, namely the variation in the resistance and reactance of the sensor for a surface crack using system of TEAM Workshop Benchmark problem, Pb. No. 15-1 (Table 1) [10]. These signals represent the signatures of crack.
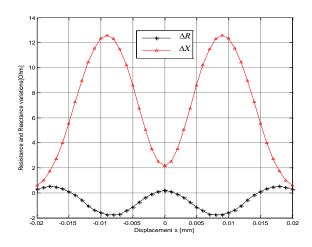

Fig. 3. Signature of the crack: the variation of resistance and reactance of the impedance of the system as function of displacement of the sensor.

IV. THE EC-NDT SIMULATION

The study of the crack size effect on the EC signal will enable us to identify the EC-NDT device sensitivity. This sensitivity allows us to define accessible parameters necessary for the inverse problem. In this respect, it will be possible to predict which relevant parameters can be calculated by the simulation.

We purposely chose to work with the same system of TEAM Workshop Benchmark problem, Pb. No. 15-1 [10]. The characteristics of this system are presented in Table 1.

Table 1: Parameters of test experiment system of TEAM Workshop Benchmark [10]

The Coil	
Outer radius	12,40 ± 0,05 mm
Inner radius	6,15 ± 0,05 mm
Height	6,15 ± 0,1 mm
Number of turns	3790
Lift-off	0,88 mm
The Test Specimen	
Conductivity	$(30,6 ± 0,20)10^6$ S/m
Thickness	12,22 ± 0,02 mm
The defect	
Length	12,6 ± 0,02 mm
Depth	5,00 ± 0,05 mm
Width	0,28 ± 0,01 mm
Others Parameters	
Frequency	900 Hz
Skin depth at 900 Hz	3,04 mm

A. Crack width effect on the EC signal

Most of previous works known to the authors were concerned with the depth effect of the crack on the EC signal, but few studies were concerned with the width effect [1] and [15].

Figure 4 depicts EC signatures of three different cracks having the identical length and depth with different widths: 0.30 mm, 0.25 mm and 0.15 mm.
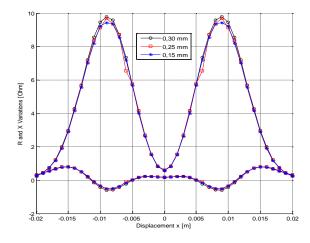

Fig. 4. EC signatures of cracks with 0.30 mm, 0.25 mm and 0.15 mm width having the identical length and depth.

Thus, a change from 0.15 to 0.30 mm in width will have no effect on the EC signals. This result is in good agreement with the work of Chen et al. and Helifa et al. on the electro-eroded slots [1] and [15]. This can be explained by the fact that the amplitude of the crack signal depends on the ratio defect volume/scanned volume. In this interval, the increase of the width raises

the volume of the defect, but the volume ratio stays weak. The sensor is then insensitive to this change. We can conclude, that for thin cracks (<0.3 mm), the change in width has no effect on the EC signal; probably, this is a reason that researchers do not speak about this parameter.

B. Crack length effect on the EC signal

Figures 5 and 6 present EC signatures of the resistance and reactance variations with respect to the sensor displacement produced by cracks of identical width (0.20 mm) and depth (5 mm) having different lengths.
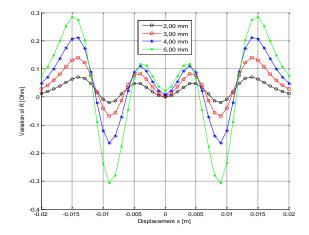

Fig. 5. Resistance vs. sensor displacement of cracks with identical width (0.20 mm) and depth (5 mm) having different lengths.
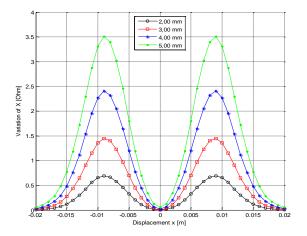

Fig. 6. Reactance vs. sensor displacement of cracks with identical width (0.20 mm) and depth (5 mm) having different lengths.

Thus, the crack length effect on the EC signal is clearly apparent contrary to the crack width. Hence, one can conclude that for thin cracks the EC signal strongly

depends on crack length.

C. Crack depth effect on the EC signal

Figures 7 and 8 show EC signatures of the resistance and reactance variations with respect to the sensor displacement produced by cracks of identical width (0.20 mm) and length (9 mm) having different depths.
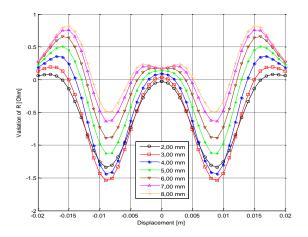

Fig. 7. Resistance vs. sensor displacement of cracks with identical width (0.20 mm) and length (9 mm) having different depths.
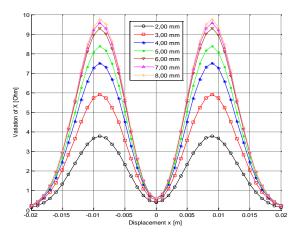

Fig. 8. Reactance vs. sensor displacement of cracks with identical width (0.20 mm) and length (9 mm) having different depths.

Thus, the crack depth effect on the EC signal is also apparent as the length effect. On the other hand, we notice that the curves of reactance vs. sensor displacement are no longer evident over a certain depth. This point will be discussed in the following paragraph.

D. EC signal and the depth limit

Figure 9 shows a zoom of three EC signatures representing the reactance variations with respect to the sensor displacement produced by cracks of identical width (0.20 mm) and length (9 mm) having different depths.
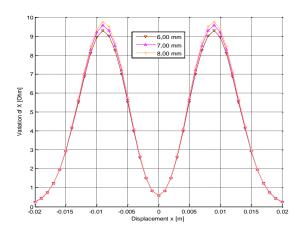

Fig. 9. Zoom on the reactance variations with respect to the sensor displacement produced by cracks of identical width (0.20 mm) and length (9 mm) having different depths.

We note in Fig. 9 that, over 6 mm depth, the curves of reactance vs. sensor displacement are no longer evident over a certain depth that we name depth limit. In consequence, we are not able to estimate the real depths of cracks exceeding these depth limit. This result corroborates the work of Helifa et al. [1].

We can also show this depth limit by plotting the reactance variations with respect to the depth of cracks at one position of sensor (Fig. 10).
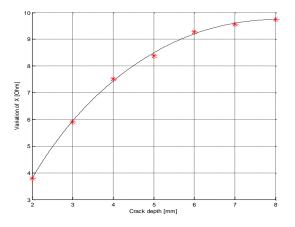

Fig. 10. Reactance vs. depth of cracks with identical width (0.20 mm) and length (9 mm) at one position of sensor.

We must note here that, this depth limit is not related to the skin depth. Indeed, the depth limit in our case is estimated at 6 mm while the skin depth is 3 mm. This can be explained by the fact that for a surface

crack, which is open to the surrounding, and as the probe radiates to an extent of many times its diameter, the electromagnetic field can, therefore, diffuse deeply inside this surface crack at distances well over than the skin depth. Eddy currents always occur at equal effective skin depth in both surface and internal walls of this crack.

We can show the same result for the resistance variations; however, the depth limit is not the same as defined for the reactance variations. Indeed, Fig. 11 shows that the curves representing the resistance variations with respect to the sensor displacement are always discernible even beyond the depth limit previously set for the reactance variations.
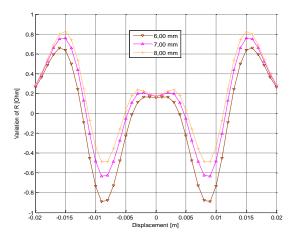

Fig. 11. Zoom on the resistance variations with respect to the sensor displacement produced by cracks of identical width (0.20 mm) and length (9 mm) having different depths.

Figure 12 shows the resistance variations with respect to the depth of cracks at one position of sensor.
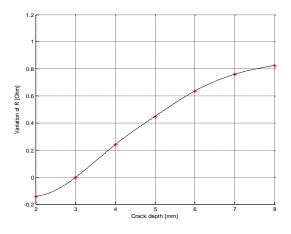

Fig. 12. Resistance vs. depth of cracks with identical width (0.20 mm) and length (9 mm) at one position of sensor.

Thus, Figs. 9, 10, 11 and 12 show that the depth limit is not the same for the resistance and reactance variations.

In conclusion, and in spite of the fact that signals corresponding to resistance variations are much less intense than those of the reactance variations, the resistance variations are more sensitive to the crack depth than the reactance ones.

V. DATA INVERSION

The next step consists of inversion of data results, using neural networks (NN) based MLP (*MultiLayer Perceptron*) model. There are two reasons to this choice. The first one is that, NN are able to approximate any function with a finite number of discontinuities to any required precision, they are "universal parcimonial approximators". The second reason is that, NN are known to be fast in finding quasi-instantly the solution of nonlinear problems.

To solve the inverse problem, it is necessary to achieve the Hadamard conditions [14]. Instead of using one numerical measurement only corresponding to a single position, we will use the crack signature which contains a whole set of numerical measurements corresponding to a set of sensor positions. We choose as input of NN a vector containing 21 numerical measurements of the resistance variation related to 21 different sensor positions through the surface crack. Indeed, the shapes of curves in Fig. 13 cannot be represented by only 2 or 3 values of the resistance variation. Thus, with this approach we can overcome the unicity problem of solution. Indeed, a cross over points in Fig. 13 are a tangible proof of the fact that the input vector NN containing 2 or 3 values is not sufficient to define completely a single crack as is often done in many works [2].
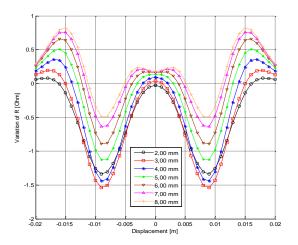

Fig. 13. Resistance vs. sensor displacement of cracks with identical width (0.20 mm) and length (9 mm) having different depths.

A. NN MLP inversion

Behavioral laws of EC sensors are strongly non-linear. There are NN structures able to model these types of problems. Among these structures, the multilayer neural networks MLP (or Multilayer Perceptron) are the most common and widely used in the EC NDT [2] and [16]. We use the algorithm of back-propagation gradient of Levenberg-Marquardt, adopted for multilayer networks with a supervised learning [2].

Since all our input parameters have the same physical unit (impedance), we do not need preconditioning. This is also the case for output parameters (length). Furthermore, the EC crack signature is already centered and does not need any further centering.

B. Characterization of surface cracks

The objective consists of simultaneously estimating the two main crack parameters: length and depth. The response of EC sensor simulated by 3D Finite elements is the data base for the NN.

The structure of NN application is made of hidden layer with hyperbolic tangent activation function and an output layer with a linear activation function (Fig. 14). The number of neurons in the hidden layer is equals to 80.
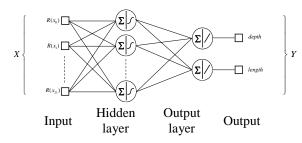

Fig. 14. Implementation of the MLP NN.

C. Result validation

The last step is to test the model's ability to be generalized. In this phase, we will test the network capacity to find the target parameters (crack depth and length) corresponding to examples of impedances in the learning domain. These examples are different from those used in the two basis previously used for learning and evaluation.

The relative error between the real parameters and the estimated ones is characterized for each P parameter using the following relationship:

$$ER(P) = \sqrt{\frac{1}{N} \sum_{i=1}^{N} \left(\frac{P_i - P_i}{P_i} \right)^2}, \qquad (3)$$

where N, P_i and P_i are respectively the number of examples over the test basis, the desired parameters and the estimated parameters of the NN.

Table 2 shows the relative errors in estimating the crack parameters (length and depth) by the NN MLP method.

Table 2: Relative errors by the NN MLP method

	Depth	Length
Relative error by NN MLP	2,50%	2,00%

When using NN, the training phase determines the limitations. That means following the interval values [min, max] of inputs and outputs sets, the performance of NN depends on this interval. For larger intervals the limitations will evolve.

According to the obtained results, we can conclude that the inverse model by MLP NN is able to generalize and gives results with good accuracy. This aptitude of generalizing is illustrated in Figs. 15 and 16.
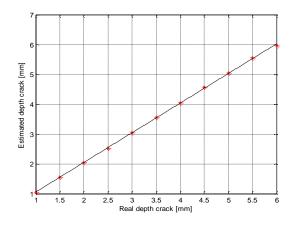

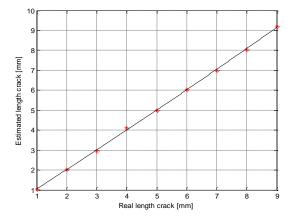Fig. 15. Estimated depth vs. real depth of crack.

Fig. 16. Estimated length vs. real length of crack.

VI. CONCLUSION

During this work, the 3D finite element simulation of the EC NDT for a surface crack was conducted. The simulation results were validated and compared to those given by the Team Workshop Benchmark problem, Pb. No. 15-1. This study shows that for thin cracks, the EC

signal is independent of the crack width. However, it strongly depends on its length and depth. Nevertheless, beyond a certain depth limit, the sensor becomes insensitive beyond this limit. The depth limit is not related to the skin depth and can reach much higher values than that of skin depth.

The inverse problem is solved using an MLP neural networks. The application consists to simultaneously estimate the two parameters of the crack: depth and length. The use of a range of variation values of resistance or reactance (signature of the crack) is taken as input vector for MLP NN. The generalized approach that we developed can estimate with good accuracy the crack required geometric parameters.

REFERENCES

[1] B. Helifa, A. Oulhadj, A. Benbelghit, I. K. Lefkaier, F. Boubenider, and D. Boutassouna, "Detection and measurement of surface cracks in ferromagnetic materials using eddy current testing," *NDT&E International, Elsevier*, vol. 39, issue 1, pp. 384-390, Mar. 2006.

[2] Y. Le Bihan, J. Pavo, and C. Marchand, "Characterization of small cracks in eddy current testing," *Eur. Phys. J. Appl. Phys.*, 43, pp. 231-237, 2008.

[3] D. Prémel and A. Baussard, "Eddy-current evaluation of three-dimensional flaws in flat conductive materials using a Bayesian approach," *Institute of Physics Publishing*, Inverse Problems 18, pp. 1873-1889, 2002.

[4] G. Rubinacci, A. Tamburrino, and S. Ventre, "Regularization and numerical optimization of a fast eddy current imaging method," *IEEE Transactions on Magnetics*, vol. 42, no. 4, pp. 1179-1182, Apr. 2006.

[5] B. Helifa, A. Zaoui, M. Feliachi, I. K. Lefkaier, F. Boubenider, and A. Cheriet, "Simulation du CND par courants de Foucault en vue de la caractérisation des fissures débouchantes dans les aciers austénitiques," *6ème Conférence Européenne sur les méthodes numériques en Electromagnétisme NUMELEC*, Liège – Belgique, Déc. 2008.

[6] X. Qiu, P. Zhang, J. Wei, X. Cui, C. Wei, and L. Liu, "Defect classification by pulsed eddy current technique in con-casting slabs based on spectrum analysis and wavelet decomposition," *Sensors and Actuators A: Physical*, 20, pp. 272-281, 2013.

[7] R. Smid, A. Docekal, and M. Kreidl, "Automated classification of eddy current signatures during manual inspection," *NDT&E International*, vol. 38, pp. 462-470, 2005.

[8] L. Udpa, P. Ramuhalli, J. Benson, and S. Udpa, "Automated analysis of eddy current signals in steam generator tube inspection," *16th WCNDT World Conference on NDT*, Montreal, Aug. 30 – Sep. 3, 2004.

[9] G. Chen, Y. Yoshida, K. Miya, and M. Uesaka, "Application of eddy current testing inspection to the first wall of fusion reactor with wavelet analysis," *Fusion Engineering and Design*, 29, pp. 309-316, 1995.

[10] Team Workshop Problem 15, *Rectangular Slot in a Thick Plate: a Problem in Nondestructive Evaluation*, http://www.compumag.org/jsite/images/stories/TEAM/problem15.pdf.

[11] M. Rachek and M. Féliachi, "3-D movement simulation techniques using FE-methods: application to eddy current non-destructive testing," *NDT&E international, Elsevier*, vol. 40, issue 1, pp. 35-42, Jan. 2007.

[12] C. Geuzaine, *Meshing Software*, www.geuz.org/gmsh.

[13] B. Bendjima, K. Srairi, and M. Féliachi, "A coupling model for analysing dynamical behaviors of an electromagnetic forming system," *IEEE Transactions on Magnetics*, vol. 33, no. 2, pp. 1638-1641, Mar. 1997.

[14] Z. Chen, M. Rebican, N. Yusa, and K. Miya, "Fast simulation of ECT signal due to a conductive crack of arbitrary width," *IEEE Transactions on Magnetics*, vol. 42, no. 4, pp. 683-687, Apr. 2006.

[15] Ph. Beltrame and N. Burais, "Generalization of the ideal crack model in eddy-current testing," *IEEE Transactions on Magnetics*, vol. 40, no. 2, pp. 1366-1379, Mar. 2004.

[16] N. Yusa, W. Cheng, Z. Chen, and K. Miya, "Generalized neural network approach to eddy current inversion for real cracks," *NDT&E International 35*, pp. 609-614, 2002.

Bachir Helifa received the degree of High Studies (Master of Science) in Physics from USTHB University of Algiers and the Magister in Materials Sciences from Laghouat University and the Ph.D. in Materials Physics from USTHB University of Algiers. His research interests include the Materials Sciences, Non-destructive Testing, Magnetism and Electromagnetism.

Mouloud Feliachi received the Engineering degree in Electrical Engineering from the National Polytechnic School of Algiers and the Doctor Engineer degree from the Conservatoire National des Arts et Métiers of Paris and the Ph.D. in Physical Sciences from

the National Polytechnic Institute of Grenoble. His research interests include Modelling of Electromagnetic Systems, Non-destructive Testing and Magnetic materials.

Ibn Kheldoun Lefkaier received the degree of High Studies (Master of Science) in Physics from Ferhat Abas University of Setif-Algeria and the Ph.D. in Solid Physics from Kabarino Balkarie University of Nalchik-Russia. His research interests include the Materials Sciences, thermodynamics of solid and Non-destructive Testing.